

# Increasing Frequency Capability of PMSM Vector Controlled Drive for Pumped Storage

Ioan Ducar, Corneliu Marinescu

\* Transilvania University/Electrical Engineering and Applied Physics, Brasov, Romania

ioan.ducar@unitbv.ro, corneliu.marinescu@unitbv.ro

**Abstract**— The subject of this paper is a comparative study between two supply modes of a permanent magnet synchronous motor (PMSM). The goal is to obtain a better efficiency for a hydraulic pump drive system. The machine (PMSM) is operated in vector control mode. The inverter is controlled with a sinusoidal pulse-width modulation (SPWM) technique. The study will allow to increase the root mean square (RMS) of the voltage and hence speed, avoiding over-modulation. The comparison is also made between third harmonic injection and over-modulation.

## I. INTRODUCTION

Renewable energy sources (RES) in most cases provide variable power. To operate efficiency, a pump driven by a PMSM supplied from RES will operate at variable speed. However, RES requires the introduction of an energy storage system (batteries, super-capacitor, flywheels or pumped storage).

Induction motor based pumping systems can obtain satisfactory efficiency at variable speed. For this, several methods have been considered to control the drive [1]. In practice, they use different motors and are designed to increase the performance. These applications were made to obtain a better overall efficiency [2, 3]. Various solutions of modern inverters have been applied for the same purpose [4].

An application at variable load requires precise control of speed and a good dynamic response. The drive can operate in semi-closed or closed loops control. For this, it requires a performing control algorithm, which sometimes increases the price of the entire equipment. It is very important a good dynamic speed and torque response. Synchronous resolver or optical encoders are used to measure the speed and rotor position. There are three control loops functioning simultaneously, to achieve: speed control, torque control and rotor positions control of the pump drive [5, 6].

This paper explores the possibility of improving efficiency by using a PMSM.

In this case, the adjusted control variable in the speed of the motor ( $\omega_r$ ). This is compared with a reference value ( $\omega_r^*$ ). The error obtained is applied to a proportional integrator (PI) controller. The controller will ensure zero error in steady state regime. The output value of the speed controller is the stator current vector ( $i_q^*$ ). The result is compared with the measured value and applied to a current regulator, a PI controller. The result will give the reference voltage, which is applied to the voltage controlled inverter [7].

Speed is controlled by electromagnetic torque. Torque is controlled by the active component of the current. D-q axis current are controlled by the voltage closed loop. The control algorithm has to compensate the coupling between the two axes and the component due to induced electromagnetic force (emf) [8].

Fig. 1 shows the block diagram of the system in autonomous mode. The supply of the pump motor group can be made from any RES. The converter ensures power transfer between the autonomous micro-grid and the PMSM. When energy demand is low, the extra electricity generated will be used to pump water from the in the upper basin. In periods when power consumption is high, the potential energy of water from the upper basin will be transformed into electricity [9].

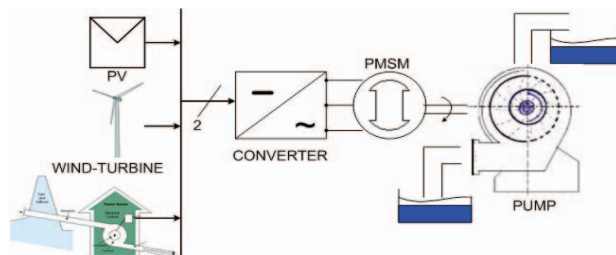


Fig. 1. Block diagram of the autonomous pumping system.

The paper is structured as follows: the second section shows the drive control principle. Third section is dedicated to the inverter control principle. The fourth section describes the simulation results. The final section is devoted to conclusion.

## II. DRIVE CONTROL PRINCIPLE

The Scalar control at variable speed of drives cannot achieve performance of the vector control one. Through the d-q model of the machine a simplified mathematical model of the PMSM was built. Separating the control active component ( $i_q$ ) from the reactive component ( $i_d$ ) two control loops can be obtained: the reactive loop, which allows the control of magnetic components (flux or stator current) and the active loop, which allows control of mechanical components (position and/or speed of the rotor and/or electromagnetic torque and stator current active component  $i_q$ ).

The resulting air gap flux consists of a flux which is obtained by pulsation (electromagnetic induction) and one obtained through the rotor permanent magnetic field, considered constant.

### A. Current controller

Current regulator design requires knowledge of closed loop transfer function. In the Fig. 2 a, b the block diagrams of PMSM in d-q coordinates are presented [10]. The PMSM equations presented given in d-q coordinate system are:

$$\begin{aligned} u_d &= R_s \cdot i_d + L_d \cdot \frac{di_d}{dt} - \omega \cdot \Psi_q \\ u_q &= R_s \cdot i_q + L_q \cdot \frac{di_q}{dt} + \omega \cdot (\Psi_d + \Psi_{PM}) \end{aligned} \quad (1)$$

where  $L_d$ ,  $L_q$ ,  $i_d$ ,  $i_q$  are the inductances and currents in d-q frame,  $R_s$  is the winding resistance,  $\omega$  is the angular velocity and  $\Psi_d$ ,  $\Psi_q$ ,  $\Psi_{PM}$  are the stator linkage fluxes due load and permanent magnet flux.

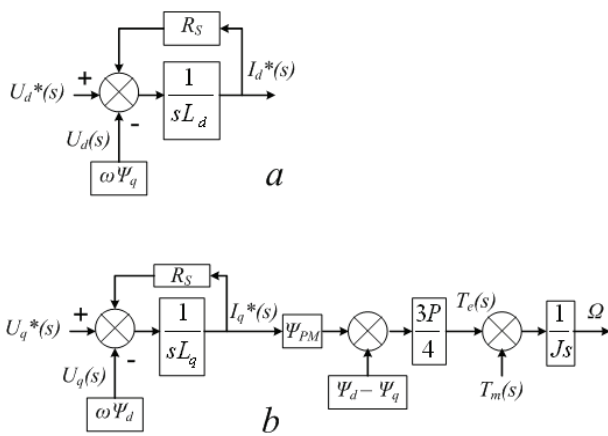


Fig. 2. Block diagram of PMSM in d-q axis.

The transfer function between component  $i_d$  and input voltage  $u_d$  in d-axis is:

$$\frac{I_d(s)}{U_d(s)} = \frac{1}{1 + \frac{R_s}{sL_d}} = \frac{1}{sL_d + R_s} = \frac{1}{1 + \frac{R_s}{sL_d}} \quad (2)$$

Similarly the transfer function in q axis was obtained. The ratio of the output size ( $I^*$ ) and input size ( $U^*$ ) defines the transfer function ( $Y$ ). The transfer function in d-q frame can be rewritten as follows:

$$\begin{cases} Y_d(s) = \frac{K_a}{1 + sT_{a-d}} \\ Y_q(s) = \frac{K_a}{1 + sT_{a-q}} \end{cases} \quad (3)$$

where  $K_a$  is the controller gain,  $T_{a-d}$  and  $T_{a-q}$  are the time constants.

In the Fig. 3 a, b diagrams of closed loop power control in d-q coordinate system are shown. If the d axis current regulator has zero reactive components, then the flux created will be that of permanent magnets. PI transfer function in axis d is:

$$\frac{I_d(s)}{I_d^*(s)} = \frac{K_{id}(1 + sT_{id})K_a}{1 + \frac{K_{id}(1 + sT_{id})K_a}{sT_{id}(1 + sT_{a-d})}} = \frac{1}{1 + \frac{sT_{id}}{K_{id}K_a}} \quad (4)$$

where  $K_{id}$ ,  $T_{id}$  are the controller gain and time constant in the d-axis.

In the same way the transfer function in q-axis was obtained. The sampling period of the system is given by the carrier signal frequency SPWM modulator. This is limiting transistor switching characteristics of power inverter to 10 kHz. This will result in a maximum sampling period of 100  $\mu$ s. The q-axis controller time constant is chosen four times the sampling period [11].

$$K_{iq} = \frac{L_q}{4 \cdot T_s} \quad (5)$$

where  $T_s$  is the sampling period. Similarly the d-axis parameter was obtained.

### B. Speed controller

The PMSM speed closed-loop diagram includes a filtering block on the input of demanded speed (Fig. 4), which compensates the speed overshooting.

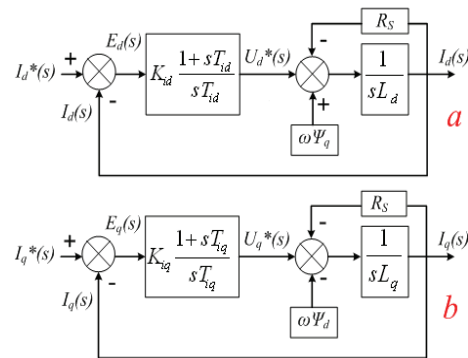


Fig. 3. Current loop of PMSM in d-q axis.

To design the speed controller transfer function the reference function is compared with the ideal one of the same order.

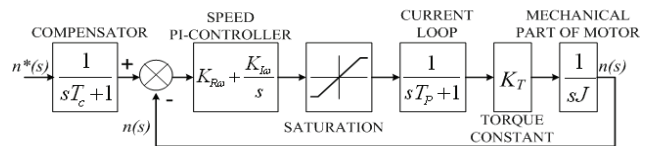


Fig. 4. Speed loop of PMSM in q-axis.

where  $T_p$  is the time constant of the current loop and  $T_c$  is the compensator time constant.

In Fig. 5 is shown a block diagram of the PMSM drive control. For the feedback loop, beside the winding currents, information about the position and the rotor speed are available. This information is obtained by means of the optical encoder. The outputs are processed to obtain the angle and the rotor speed.

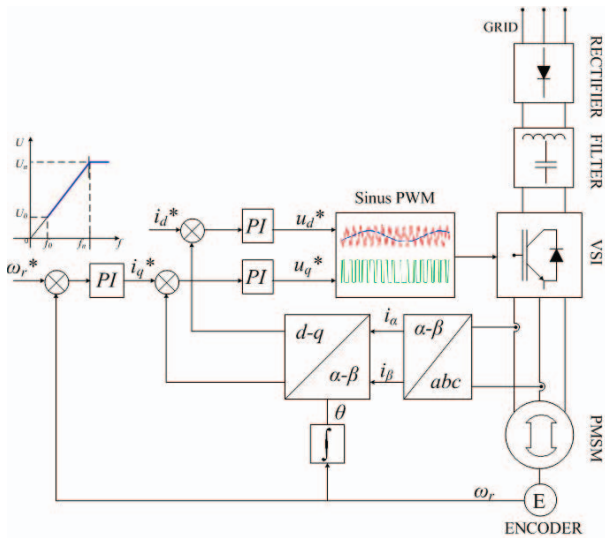


Fig. 5. Block diagram of the PMSM drive.

$$T_c = \frac{K_{R\omega}}{K_{I\omega}}, \quad (6)$$

where  $K_{R\omega}$ ,  $K_{I\omega}$  are the PI speed controller gain constant. The PI speed loop controller transfer function is:

$$\frac{n(s)}{n^*(s)} = \frac{\left(K_{R\omega} + \frac{K_{I\omega}}{s}\right) \left(\frac{1}{sT_p + 1}\right) \left(\frac{K_T}{sJ}\right)}{1 + \left(K_{R\omega} + \frac{K_{I\omega}}{s}\right) \left(\frac{1}{sT_p + 1}\right) \left(\frac{K_T}{sJ}\right) (sT_c + 1)}. \quad (7)$$

### III. INVERTER CONTROL PRINCIPLE

In the Fig. 6 is shown a schematic diagram of power inverter-motor circuit.

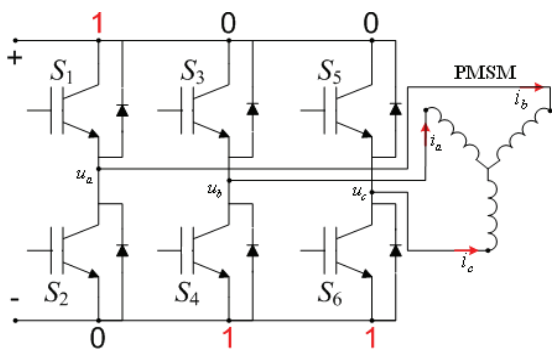


Fig. 6. Inverter-motor principle diagram.

#### A. Inverter control without third harmonic injection.

Sinusoidal reference signal is limited by the carrier. When sinusoidal signal amplitude exceeds the amplitude of the carrier signal over-modulation occurs. This phenomenon allows higher harmonics appearance.

When the modulation factor is higher than one, then control of the output voltage of the inverter cannot be done. Therefore, the resulting voltage will be distorted by harmonics.

Reference signal amplitude  $U_{ref}$  cannot exceed the amplitude signal  $U_{gen}$ . If such event occurs, the inverter will go into over-modulation. The energy absorbed from the power supply is not consumed properly. Modulated signal on the three phases are treated separately. However, loss of power increases, because of the high harmonics of the PWM signal.

The load of the voltage inverter can be a three-phase motor. Through the series inductance of the motor winding voltage PWM signal is filtered. For the resulting current to be sinusoidal, line voltages must be sinusoidal. In many power circuits, between the inverter and the motor is attached a low pass filter. The filter role is to limit higher harmonics generated by the PWM signal.

#### B. Inverter control with third harmonic injection.

When the modulation factor is high, the reference signal is injected with the third order harmonic. This method is appropriate to use DC power supply of the inverter. This could increase the output frequency corresponding to the same voltage and thus the hydraulic pump output. Injected signal amplitude is 1/3 of fundamental component. This will produce an output amplitude improvement by 15.5 %, avoiding over-modulation [12, 13].

Third order harmonic injection is done by the load neutral, ZSS (Zero Sequence Signal injection). Block diagram of TRIPWM sinusoidal signal injected into neutral is shown in the Fig. 7. ZSS signal is obtained from the signals of the three phase PWM through a power unit. The signal applied to the PWM generator is composed from a fundamental component and third harmonic component, (Fig.8).

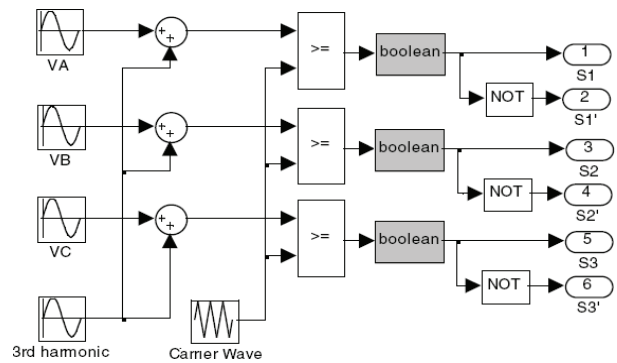


Fig. 7. The computation block diagram of injected sinusoidal signal

The RMS value of the inverter output voltage can be increased by adding third harmonic modulated signal [9]. Relationships calculations are:

$$\begin{cases} u_a = \frac{2}{\sqrt{3}} \cdot \left[ \sin(\omega t) + \frac{1}{6} \cdot \sin(3\omega t) \right] \\ u_b = \frac{2}{\sqrt{3}} \cdot \left[ \sin\left(\omega t - \frac{2\pi}{3}\right) + \frac{1}{6} \cdot \sin(3\omega t) \right] \\ u_c = \frac{2}{\sqrt{3}} \cdot \left[ \sin\left(\omega t - \frac{4\pi}{3}\right) + \frac{1}{6} \cdot \sin(3\omega t) \right] \end{cases} \quad (8)$$

Another method (TRIPWM) is Carrier-based PWM with Offset Addition (Fig. 9). The offset addition PWM scheme follows the same principle as that of third-harmonic injection. This is reducing the peak of the modu-

lation signal and hence increasing the modulation index. The output voltage magnitude reaches the same value as that of the third-harmonic injection PWM.

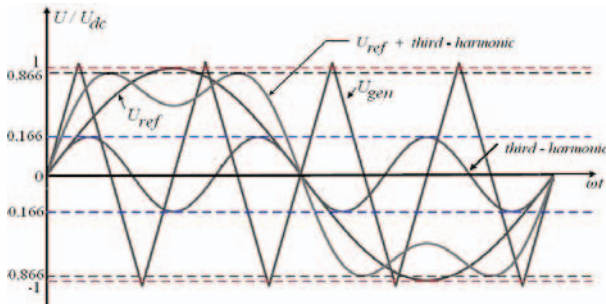


Fig.8. Waveforms for the third harmonic injection.

Another technique consists in using triangular signal. Triangular signal method is simpler compared to the injected sinusoidal (Fig.10). Relationships calculations of this method are:

$$\begin{cases} u_a = U_m \cdot [\sin(\omega t) - 0.5 \cdot (U_{\max} + U_{\min})] \\ u_b = U_m \cdot [\sin(\omega t - 2\pi/3) - 0.5 \cdot (U_{\max} + U_{\min})] \\ u_c = U_m \cdot [\sin(\omega t - 4\pi/3) - 0.5 \cdot (U_{\max} + U_{\min})] \end{cases} \quad (9)$$

where  $U_m$  is amplitude signal value and  $U_{\max}$ ,  $U_{\min}$  are  $\text{Max}\{u_a, u_b, u_c\}$  and  $\text{Min}\{u_a, u_b, u_c\}$ .

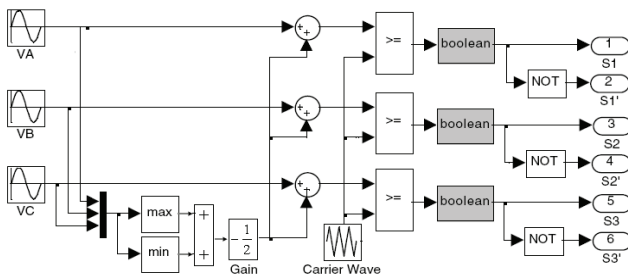


Fig. 9. The block diagram of offset addition PWM.

The calculation method (ZSS) consists in determining the minimum signal amplitude of the three signals modulators. This signal is then scaled by 0.5 and is ZSS.

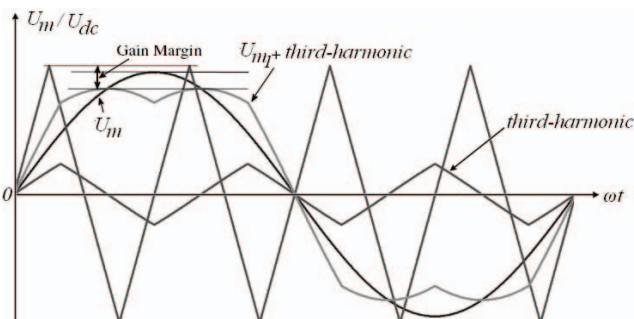


Fig. 10. ZSS method by injecting a triangular signal.

Also, a comparison between the two methods described above was made. By using them, it was found that the efficiency of the studied system does not change. Therefore, the first method was used.

#### IV. SIMULATION RESULTS

The results were obtained using the scheme from Fig. 5, which was modeled in Matlab Simulink. To simplify the calculation, a linear speed reference feature was used (Fig. 11). Reference component in d-axis is zero. In table I are presented the results obtained from simulation and rated value for several PMSMs.

The SPWM algorithm does not allow full use of the DC-link circuit voltage by the inverter. It can be seen (Fig.11) how many per cent may be used in the DC-link circuit voltage.

The characteristics shown in Fig. 12 were made considering the third harmonic injection. In Fig. 13 are shown features without third harmonic injection. Characteristic of efficiency data were obtained from simulations made in steady state.

TABLE I. VALUES RESULTS

Rated Values					Without third harmonic		
$P_m$	$U_{line}$	$I_{line}$	$U_{DC}$	$\eta$	$f$	$P_m$	$U_{DC}$
[kW]	[V]	[A]	[V]	[%]	[Hz]	[kW]	[V]
5.5	369	9.3	520	93	43.59	3.64	86.36
15	360	26	508	94	43.81	10.06	84.23
30	377	50	532	94.2	43.81	20.13	88.20
55	354	97.5	496	94.3	43.85	37.03	82.81
75	358	132	501	94.6	43.55	51.09	83.67

In table II are shown the results obtained for the 75 kW machine. At low speeds the centrifugal pump efficiency is low. By increasing the speed (frequency of motor) one can see a consistent increase in efficiency. For high power motor pump groups, increasing efficiency by one or two percent is very important.

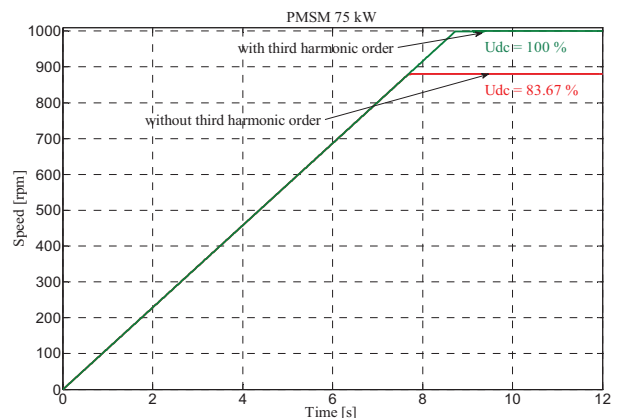


Fig. 11. Characteristics of speed depending on time

The data from the tables were obtained using the following steps:

1. Motor shaft torque and mechanical power were determined for each speed by measurements in Matlab Simulink model of the motor.

2. Then the currents, voltages and active power were measured in Simulink.
3. The power factor was computed using the above measurements.
4. The electromagnetic power was computed.
5. The difference between the active power and the electromagnetic power are gives the stator losses (electrical and magnetic losses). In the computation the optimal working temperature 75 °C for PMSM was considered.
6. Once stator electrical losses obtained magnetic losses were separated. By using the above results, the mechanical losses were computed.

The results were determined for PMSMs with power ranging from 5.5 to 75 kW.

TABLE II. PMSM 75 KW

Without third harmonic			With third harmonic			
f	$U_{a\_RMS}$	$\eta_1$	f	$U_{a\_RMS}$	$\eta_2$	$\Delta\eta$
[Hz]	[V]	[%]	[Hz]	[V]	[%]	[%]
4.297	17.05	67.148	5	19.84	70.423	3.27
8.594	34.143	80.191	10	39.74	82.427	2.23
12.891	51.28	85.684	15	59.7	87.347	1.66
12.297	68.831	88.723	20	79.74	89.977	1.25
21.615	86.242	90.577	25	99.88	91.586	1
25.954	103.74	91.822	30	120.1	92.652	0.82
30.325	121.41	92.704	35	140.6	93.393	0.68
34.711	139.33	93.352	40	161.4	93.923	0.57
39.092	157.61	93.839	45	182.5	94.317	0.47
43.552	176.26	94.211	50	204.1	94.604	0.39

## V. CONCLUSIONS

The SPWM algorithm does not allow full use of the DC voltage (Fig. 12). How many percent were used in line voltage are shown in Table I.

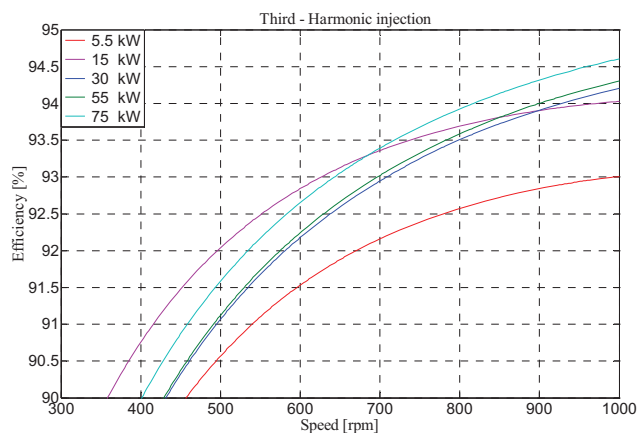


Fig. 12. Characteristics with the third harmonic injection.

In the third order harmonic injection method case the effective value of the voltage will be higher by 10-17 %. The efficiency is increasing by 3.27 % (Table II). As a result, the voltage of the DC circuit can be used completely.

The red line in Fig. 13 shows up where the PMSMs without injecting third harmonic could be used. When the third harmonic injection was made, at speed over 50 %, efficiency does not increase very much.

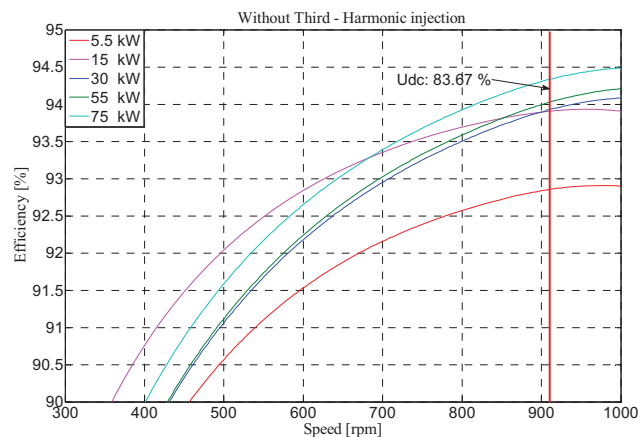


Fig. 13. Characteristic without the third harmonic injection.

## REFERENCES

- [1] A. Forcos, C. Marinescu, "Motor Pump Group Efficiency in a Wind Energy Pumped storage System," Proceedings of the International Symposium on Advanced Topics in Electrical Engineering, Bucharest, Romania, vol. 7, pp. 1-6, May 2011.
- [2] I. Ducar, C. Marinescu, "The PMSM Efficiency at Variable Speed for Pumping Application," Proceedings of the International Conference and Exposition on Electrical on Power Engineering, Iasi, Romania, October, 2014, in press.
- [3] I. Ducar, C. P. Ion, "Design of a PMSG for Micro Hydro Power Plants," Proceedings of the International Conference on Optimization of Electrical Equipment, Brasov, Romania, vol. 13, pp. 712-717, May 2012.
- [4] A. Forcos, C. Marinescu, R. Teodorescu and L. Clotea, "Efficiency Improvement for Wind Energy Pumped Storage Systems," Proceedings of International Symposium on Industrial Electronics, Gdansk, Poland, vol. 20, pp. 579-584, June, 2011.
- [5] R. Krishnan, Permanent Magnet Synchronous and Brushless DC Motor Drives, CRC Press, 2010.
- [6] I. Boldea, S. Nasar, Vestor Control of AC Drivers, CRC Press, 1992.
- [7] R. Magureanu, N. Vasile, Servomotoare fara Perii de Tip Sincron, Ed. Tehnica, 1990.
- [8] R. Krishnan, Electric Motor Drives. Modeling, Analysis and Control, Prentice Hall, 2001.
- [9] A. Forcos, C. Marinescu, Sisteme de Stocare ale Energiei Eoliene Utilizand Energia Hidroelectrica, Ed. Universitatii Transilvania, 2011.
- [10] M. Peter, M. Pavol and V. Jan, "PI-Controllers Determination for Vector Control Motion," Proceedings of the Annual Conference Technical Computing, Bratislava, Slovakia, vol. 18, pp. 70-77, October, 2010.
- [11] B. Alecsa, Sisteme Incorporate cu FPGA pentru Controlul Proceselor Rapide, Thesis, Tehnical University of Iasi, 2011.
- [12] P. Hue Tran, Matlab/Simulink Implementation and Analysis of Three Pulse-Width-Modulation (PWM) Techniques, Master Thesis, Boise State University, 2012.
- [13] I. Serban, Microretele Hibrade cu Surse Regenerabile de Energie, Ed. Transilvania University of Brasov, 2008.